ISSN 1674-1056
http://cpb.iphy.ac.cn
http://iopscience.iop.org/cpb
中国物理 B
Chinese Physics
中国物理
Chinese Physics B

# Structural, magnetic properties, and electronic structure of hexagonal FeCoSn compound

Yong Li(李勇), Xue-Fang Dai(代学芳), Guo-Dong Liu(刘国栋), Zhi-Yang Wei(魏志阳), En-Ke Liu(刘恩克), Xiao-Lei Han(韩小磊), Zhi-Wei Du(杜志伟), Xue-Kui Xi(郗学奎), Wen-Hong Wang(王文洪), Guang-Heng Wu(吴光恒)
**Citation:**Chin. Phys. B . 2018, 27(2): 026101. **doi:** 10.1088/1674-1056/27/2/026101

Journal homepage: http://cpb.iphy.ac.cn; http://iopscience.iop.org/cpb

**What follows is a list of articles you may be interested in**

---

## Uniaxial strain-modulated electronic structures of Cd*X* (*X*=S, Se, Te) from first-principles calculations: A comparison between bulk and nanowires

Linlin Xiang(相琳琳), Shenyuan Yang(杨身园)
Chin. Phys. B . 2017, 26(8): 087103. **doi:** 10.1088/1674-1056/26/8/087103

## Effect of anionic ordering on the electronic and optical properties of $BaTaO_2N$: TB-mBJ density functional calculation

K Bettine, O Sahnoun, M Sahnoun, M Driz
Chin. Phys. B . 2017, 26(5): 057101. **doi:** 10.1088/1674-1056/26/5/057101

## Electrical property effect of oxygen vacancies in the heterojunction of $LaGaO_3/SrTiO_3$

Fu-Ning Wang(王芙凝), Ji-Chao Li(李吉超), Xin-Miao Zhang(张鑫淼), Han-Zhang Liu(刘汉璋), Jian Liu(刘剑), Chun-Lei Wang(王春雷), Ming-Lei Zhao(赵明磊), Wen-Bin Su(苏文斌), Liang-Mo Mei(梅良模)
Chin. Phys. B . 2017, 26(3): 037101. **doi:** 10.1088/1674-1056/26/3/037101

## Structural, electronic, and magnetic properties of vanadium atom-adsorbed $MoSe_2$ monolayer

Ping Liu(刘萍), Zhen-Zhen Qin(秦真真), Yun-Liang Yue(乐云亮), Xu Zuo(左旭)
Chin. Phys. B . 2017, 26(2): 027103. **doi:** 10.1088/1674-1056/26/2/027103

## Band offsets engineering at $Cd_xZn_{1-x}S/Cu_2ZnSnS_4$ heterointerface

Wujisiguleng Bao(包乌吉斯古楞), Sachuronggui(萨初荣贵), Fang-Yuan Qiu(仇方圆)
Chin. Phys. B . 2016, 25(12): 0127102. **doi:** 10.1088/1674-1056/25/12/127102

---

# Structural, magnetic properties, and electronic structure of hexagonal FeCoSn compound*

Yong Li(李勇)[1,2], Xue-Fang Dai(代学芳)[1,†], Guo-Dong Liu(刘国栋)[1], Zhi-Yang Wei(魏志阳)[2], En-Ke Liu(刘恩克)[2], Xiao-Lei Han(韩小磊)[3], Zhi-Wei Du(杜志伟)[3], Xue-Kui Xi(郗学奎)[2], Wen-Hong Wang(王文洪)[2], and Guang-Heng Wu(吴光恒)[2]

[1] *School of Material Science and Engineering, Hebei University of Technology, Tianjin* 300130, *China*

[2] *State Key Laboratory for Magnetism, Beijing National Laboratory for Condensed Matter Physics, Institute of Physics, Chinese Academy of Sciences, Beijing* 100190, *China*

[3] *National Analysis and Testing Center for Nonferrous Metals & Electronic Materials, Beijing General Research Institute for Non-ferrous Metals, Beijing* 100088, *China*

(Received 27 November 2017; revised manuscript received 11 December 2017; published online 5 January 2018)

The structural, magnetic properties, and electronic structures of hexagonal FeCoSn compounds with as-annealed bulk and ribbon states were investigated by x-ray powder diffraction (XRD), differential scanning calorimetry (DSC), transmission electron microscope (TEM), scanning electron microscope (SEM), magnetic measurements, and first-principles calculations. Results indicate that both states of FeCoSn show an $Ni_2In$-type hexagonal structure with a small amount of FeCo-rich secondary phase. The Curie temperatures are located at 257 K and 229 K, respectively. The corresponding magnetizations are 2.57 $\mu_B$/f.u. and 2.94 $\mu_B$/f.u. at 5 K with a field of 50 kOe (1 Oe = 79.5775 A·m$^{-1}$). The orbital hybridizations between 3*d* elements are analyzed from the distribution of density of states (DOS), showing that Fe atoms carry the main magnetic moments and determine the electronic structure around Fermi level. A peak of DOS at Fermi level accounts for the presence of the FeCo-rich secondary phase. The $Ni_2In$-type hexagonal FeCoSn compound can be used during the isostructural alloying for tuning phase transitions.

**Keywords:** FeCoSn, hexagonal structure, first-principles calculations

**PACS:** 61.05.cp, 71.15.Mb, 75.20.En **DOI:** 10.1088/1674-1056/27/2/026101

## 1. Introduction

A class of ternary intermetallic compounds $MM'X$ was reported[1] in 1953. In this class of $Ni_2In$-type hexagonal alloys, bearing the general formula $MM'X$, they are ternary alloys of stoichiometric composition, in which $M$ and $M'$ are generally transition elements (3*d* metals) and $X$ is carbon or boron group elements. The atom site occupation rule of hexagonal $Ni_2In$-type structures is followed:[2] for the 3*d* metals of $MM'X$, atoms occupy two sublattices: atoms with less number of valence electrons tend to occupy 2*a* sites, atoms with more number of valence electrons tend to occupy 2*d* sites; the main group elements always occupy 2*c* sites. Here, 2*a*: (0, 0, 0), (0, 0, 1/2), 2*d*: (1/3, 2/3, 3/4), (2/3, 1/3, 1/4), 2*c*: (1/3, 2/3, 1/4), (2/3, 1/3, 3/4).

In $MM'X$ family, MnNiGe,[3–6] MnCoGe,[7] MnCoSi,[8] MnNiSi[3,9] were reported on, that first-order phase transitions happen from $Ni_2In$-type hexagonal to TiNiSi-type orthorhombic structures while many other members have no structural transitions. Recently, many efforts were carried out to couple the magnetic and structural transitions in $MM'X$ alloys and to further tailor the magnetic martensitic transitions aiming at promoting magnetoresponsive effects, such as ferromagnetic shape memory effect, giant magnetocaloric and magnetoelastic effects.[10–16] In particular, a method of isostructural alloying was proposed to realize the materials design, in which two compounds with the same crystal structure (members of $MM'X$ family) but with different properties (e.g., martensitic transition temperature, magnetic ordering temperature), respectively, are selected and used to determine the proper alloying (doping) elements. MnNiGe undergoes a martensitic transition at 470 K and has a Néel temperature $T_N^M = 346$ K in the martensitic state, Curie temperature $T_C^A = 205$ K in the austenitic state. Liu *et al.*[11] successfully established Curie temperature windows (CTWs) to achieve magnetostructural transitions by isostructurally alloying MnNiGe with the non-transition MnFeGe and FeNiGe respectively in 2012, and with the non-transition CoNiGe in 2013. It has been approved that the structural stability and magnetism of the non-transition compounds will greatly influence the results of material design.[11–14] Subsequently, many magnetostructural transitions were gained by introducing non-transition compounds with the principle of isostruc-

*Project supported by the National Natural Science Foundation of China (Grant Nos. 51431009 and 51271038), the Joint NSFC-ISF Research Program, Jointly Funded by the National Natural Science Foundation of China and the Israel Science Foundation (Grant No. 51561145003).

†Corresponding author. E-mail: xuefangdai@126.com

© 2018 Chinese Physical Society and IOP Publishing Ltd 

tural alloying.[17–30] Therefore, the basic parameters of non-transition compounds are very important for tuning of magnetic phase-transition materials, but are seldom reported.

As a desired compound, there is little reported information about FeCoSn. In this work, we systematically study the $MM'X$ hexagonal FeCoSn compound with no structural transition. The as-annealed bulk and ribbon samples were used to tune the phase formation of this compound. The structural and magnetic properties were studied by experiments and first-principles calculations.

## 2. Experimental details

As-cast FeCoSn compound was prepared by arc-melting high-pure metals Fe (99.98%), Co (99.99%), and Sn (99.99%) in an argon atmosphere, the resultant ingots of FeCoSn were subjected to different subsequent treatments: 1) annealed at 1273 K for 5 days followed by quenching (denoted as AQ1273) and 2) using melt spinning technique to prepare ribbon sample, rotation rate is 25 m/s, subsequently annealed at 1073 K for 2 days followed by quenching (denoted as RQ1073). The crystal structures were confirmed by x-ray powder diffraction (XRD) measurements at room temperature. Differential scanning calorimetric (DSC) measurements were performed with a rate of 10 K/min to investigate the thermal property. The temperature dependence of the magnetic measurements under zero-field-cooling (ZFC) and field-cooling (FC) method were carried out by superconducting quantum interference device (SQUID) magnetometer within the temperature interval of 5 K$\sim$ 400 K and the fields up to 50 kOe. The transmission electron microscope (TEM) and scanning electron microscope (SEM) with energy dispersive spectrometer (EDS) were used to explore the microstructures. The CASTEP code[31] using the pseudopotential method with plane-wave-basis set based on the density-functional theory was applied to calculate the magnetic moments and density of states (DOS) of FeCoSn. The exchange correlation energy for the structural relaxations and the electronic structures was treated under the generalized-gradient approximation (GGA).[32] The plane-wave cutoff energy of 500 eV and 120 ($14\times14\times10$) $k$ points in the irreducible Brillouin zone were used to ensure a good convergence of the total energy.

## 3. Results and discussion

In order to investigate the structural property, room-temperature XRD patterns of FeCoSn were employed. Figure 1(a) shows the crystal structure of AQ1273 sample. The typical diffraction peaks with the Miller indices are indexed as $Ni_2In$-type hexagonal phase and the lattice constants are $a = 4.189$ Å, $c = 5.208$ Å. This indicates FeCoSn can form an isostructural $Ni_2In$-type hexagonal phase, which is important to the tuning of magnetostructural transitions in hexagonal family.[11–14] At the same time, a small amount of cubic phase is observed in the hexagonal matrix. For RQ1073 sample, the lattice constants of hexagonal structure are $a = 4.173$ Å, $c = 5.195$ Å, and cubic phase is also seen in Fig. 1(b). Compared with theoretically calculated lattice constants, $a = 4.376$ Å, $c = 5.253$ Å, the experimental lattice constants are both smaller than the value of the calculated lattice constants. The corresponding values are listed in Table 1. The results indicate that it is difficult to obtain pure hexagonal phase and the secondary phase cannot be suppressed in the stoichiometric FeCoSn. The case of hexagonal main phase with small amounts of secondary phase has also been observed in MnCoSn and FeNiGe.[1,33,34]

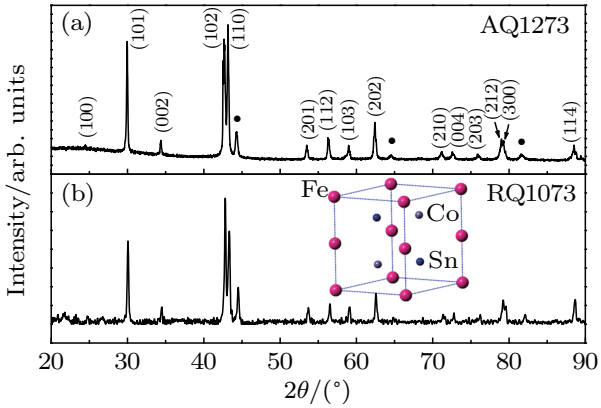



**Fig. 1.** (color online) Room-temperature XRD pattern of FeCoSn with AQ1273 (a) and RQ1073 (b), respectively. (*hkl*) denotes the Miller indices of a $Ni_2In$-type hexagonal structure and "·" represents the cubic phase, respectively. The inset shows the crystal structure and atomic site occupation of hexagonal FeCoSn.

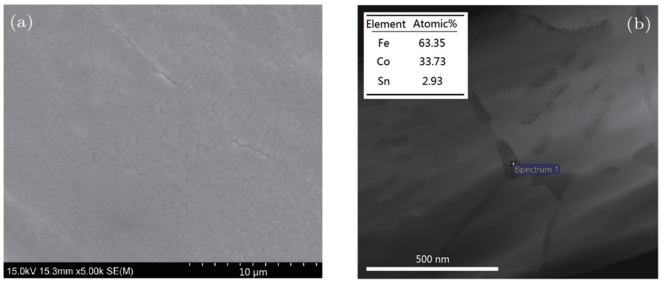



**Fig. 2.** (a) SEM image and (b) TEM image with composition analysis on the secondary phase of RQ1073 sample. The inset shows the result of EDS analysis performed at the marked point.

In Fig. 2, the SEM image and the TEM image with energy dispersive spectroscopy (EDS) of RQ1073 sample were carried out to characterize the microstructure and determine the chemical compositions, respectively. From SEM image of Fig. 2(a), the granular microstructure composed by the equiaxed crystal grains can be observed. In order to detect the secondary phase, we performed the TEM and composition analysis of EDS, as shown in the inset to Fig. 2(b). It can be

seen that the secondary phase is FeCo-rich cubic phase which locates around the grain boundaries of hexagonal main phase. The results show that the FeCo-rich phase exists in hexagonal FeCoSn compound, which is consistent with XRD analysis in Fig. 1.

Figure 3(a) shows the low-magnification TEM image of RQ1073 sample. We selected the red square area to obtain the selected area electron diffraction (SAED) pattern. The indexing of crystallographic plane along the projection plane of [001] zone axes are shown in the SAED pattern from the inset of Fig. 3(a). The secondary phase, bright area in the targeted compound, are also obviously seen. As shown in Fig. 3(b), the high-resolution (HR) TEM image from the red area in Fig. 3(a) is taken. From the HRTEM image we can see the hexagonal-ring structure clearly. The atom lines are uniformly dispersed and periodic in the *ab* plane. The metrical distance between adjacent atomic columns is calculated as 2.407 Å, and the corresponding value of lattice constant is 4.170 Å which is consistent with the value of experimental lattice constant obtained from XRD analysis ($a = 4.173$ Å) with RQ1073. The main phase crystallizes hexagonal $Ni_2In$-type structure, which is coherent with the XRD analysis.

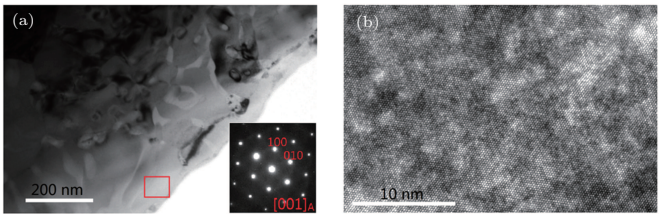



**Fig. 3.** (color online) (a) the low-energy TEM image and selected area electron diffraction (SAED) pattern (inset comes from red square area) and (b) High resolution TEM image of RQ1073 sample.

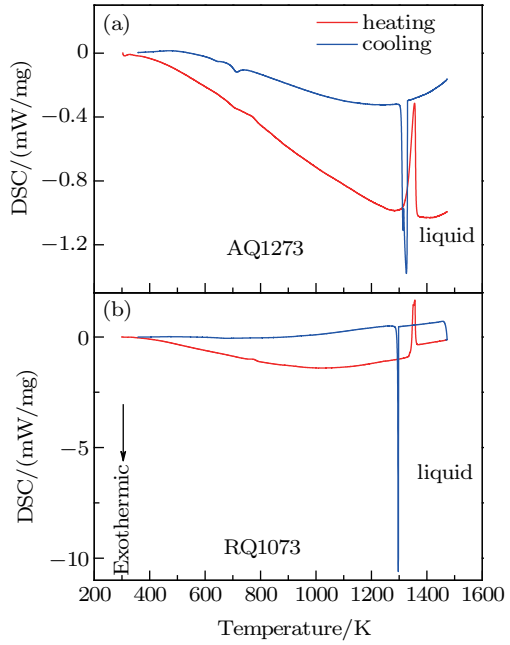



**Fig. 4.** (color online) DSC analysis for (a) AQ1273 and (b) RQ1073 samples of FeCoSn upon heating and cooling with a rate of 10 K/min.

The differential scanning calorimetric (DSC) measurements for (a) AQ1273 and (b) RQ1073 samples of FeCoSn were employed, and the corresponding curves are shown in Fig. 4. As shown in Fig. 4(a), for AQ1273 sample, a small peak and a large endothermic peak appear upon heating and corresponding exothermic peaks are also seen upon cooling. The large endothermic and exothermic peaks, namely melting and solidifying peaks, are observed at 1353 K and 1326 K, respectively. The small peaks locate at 714 K upon cooling and 768 K upon heating, which may be related to an order-disorder transition. As shown in Fig. 4(b). The melting and solidifying peaks locate at 1355 K and 1296 K, respectively and the peaks of order-disorder transition locate at 701 K upon cooling and 771 K upon heating for the RQ1073 sample. From the analysis of XRD, DSC and electron microscopy, the coexistence of two phases is maintained in a wide temperature range.

In order to investigate the magnetic properties, temperature dependence of the magnetization ($M(T)$ curves) under a magnetic field of 100 Oe and the magnetization curve as a function of applied field ($M(H)$ curves) at 5 K are measured for AQ1273 and RQ1073 samples, respectively, as shown in Fig. 5. Figures 5(a) and 5(c) show $M(T)$ curves for AQ1273 and RQ1073 samples, respectively. The samples were initially cooled in zero magnetic field and the ZFC data were collected on heating by applying a magnetic field of 100 Oe. Subsequently, the FC data were collected upon cooling without removing the applied field. For the heating process, parts of magnetic moments are frozen at low temperatures, and the magnetization increases slightly as increasing temperature firstly, and then sharply decreases when reaching the Curie temperature. For the cooling process, the magnetization curve is almost completely coincident with the curve upon heating, showing that a second-order transition happens in hexagonal austenite state, defined as Curie temperature ($T_C$). The curve cannot return to the original state at low temperatures. This irreversible splitting happens during heating and cooling curves in the vicinity of 200 K for both AQ1273 and RQ1073. The Curie temperatures (listed in Table 1) locate at 251 K (Fig. 5(a)) and 229 K (Fig. 5(c)) for AQ1273 and RQ1073, respectively. We also notice that the values of magnetization above $T_C$ are not zero, suggesting that the FeCo-rich phase indeed exists in ferromagnetic state. A typically ferromagnetic $M(H)$ curve is observed for either AQ1273 sample or RQ1073 sample, as presented in Figs. 5(b) and 5(d). It is found that the saturation fields are both about 1 kOe (relatively low) and the saturation magnetizations in 50 kOe are 2.57 $\mu_B$/f.u. and 2.94 $\mu_B$/f.u. for AQ1273 and RQ1073 respectively. In addition, the values are smaller than theoretical calculations due to the secondary phase.

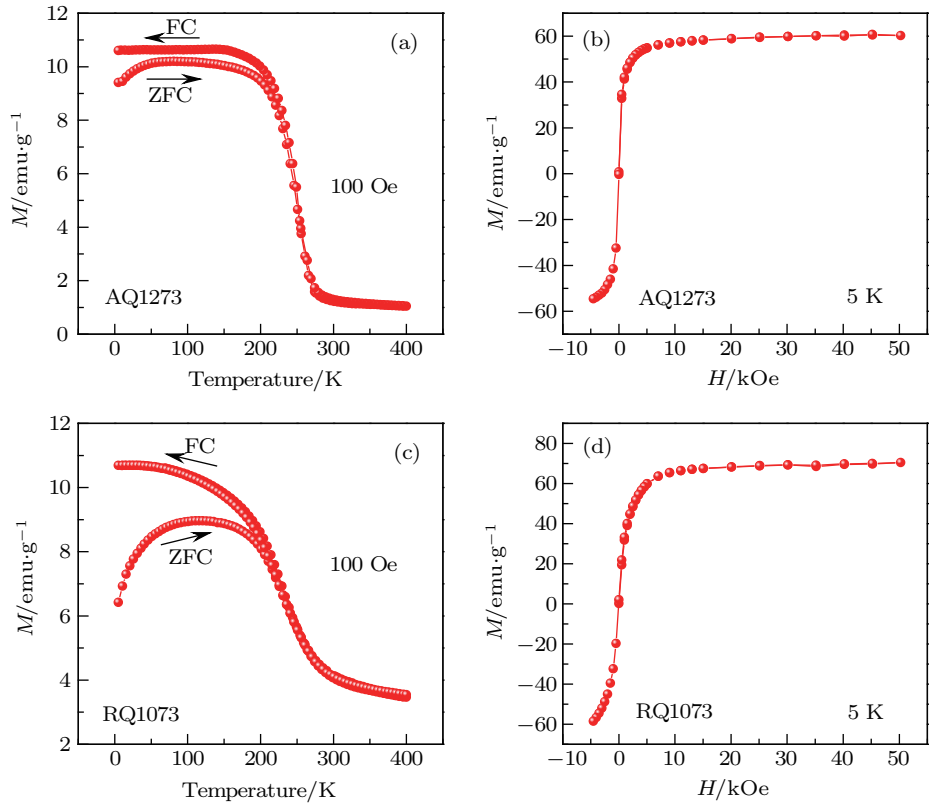



**Fig. 5.** (color online) (a) and (c) Temperature dependence of the magnetization ($M(T)$ curves) with ZFC-FC method under a magnetic field of 100 Oe for AQ1273 and RQ1073 samples, respectively; (b) and (d) Magnetization curve as a function of applied field at 5 K for AQ1273 and RQ1073 samples, respectively.

**Table 1.** The experimental and theoretically calculated parameters of hexagonal FeCoSn.

| | Experiments | | Calculations |
|---|---|---|---|
| | AQ1273 | RQ1073 | |
| $a$/Å | 4.189 | 4.173 | 4.376 |
| $c$/Å | 5.208 | 5.195 | 5.253 |
| total $M/\mu_B$ | 2.57 | 2.94 | 3.17 |
| $M_{Fe}/\mu_B$ | – | – | 2.56 |
| $M_{Co}/\mu_B$ | – | – | 0.76 |
| $M_{Sn}/\mu_B$ | – | – | 0 |
| $T_C$/K | 251 | 229 | – |

The first-principles calculations were performed to investigate the magnetic moments and density of states (DOS). Figure 6 shows the total and partial densities of states (DOSs) of stoichiometric FeCoSn. There are strong $d$–$d$ orbital hybridizations between Fe and Co atoms from −4 eV to +2 eV. In spin-up state, the hybridization peaks appear at −2.9 eV and −1.6 eV and in spin-down state the hybridization peaks appear at −1.9 eV, −1.0 eV, and 0.3 eV. A strong $p$–$d$ orbital hybridization can be observed around −4 eV between Co and Sn atoms in both spin states. Furthermore, it can be seen that for Fe atom, the spin-down DOS mainly locates above the Fermi level, while the spin-up DOS mainly locates below the Fermi level. This results in a large spin splitting in two spin states and a large net magnetic moment (2.56 $\mu_B$, see Table 1) on Fe atoms. Compared with the Fe atom, the Co atom shows a relatively weak spin splitting with more spin-down states being occupied. The Co atom thus carries a smaller moment (0.76 $\mu_B$, see Table 1). In the total DOS the low energy region below −5 eV consists mainly of $p$ electrons of the Sn

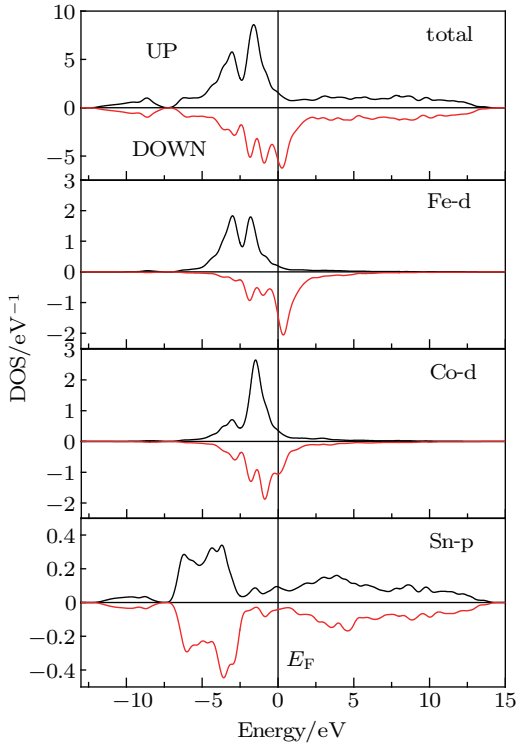



**Fig. 6.** (color online) The total and partial densities of states (DOSs) of stoichiometric FeCoSn.

atoms. From the DOS distribution of FeCoSn, it can be seen that *p–d* hybridization between Co–Sn atoms serves mainly as covalent networks, while Fe atoms are surrounded by covalent networks, carrying the main magnetic moments and determining the electronic structure around Fermi level. Strikingly, a peak of DOS of Fe atoms appear around Fermi level in spin-down state, which may lead to instability of the system. The presence of the FeCo-rich second-phase in stoichiometric FeCoSn may be attributed to this peak.

To clearly show the magnetic moments of each atom, the magnetization distribution and the spin electron density pattern in stoichiometric FeCoSn compound are depicted in Fig. 7. The main group element Sn does not carry magnetic moments. The scale bar from blue to red corresponds to increasing spin electron localization. Strong localization of (positive) spin electron density values (magnetization distribution) exist around Fe atoms, indicating that Fe atoms carry significant localized moments. Considerable but lower spin electron density values are observed for Co atoms, due to its strong *p–d* hybridization with Sn atoms. These results are in good agreement with the conclusion from DOS. In FeCoSn, the magnetizations, mainly originating from Fe and Co moments, keep high and stable values, which is common in other $MM'X$ alloys.

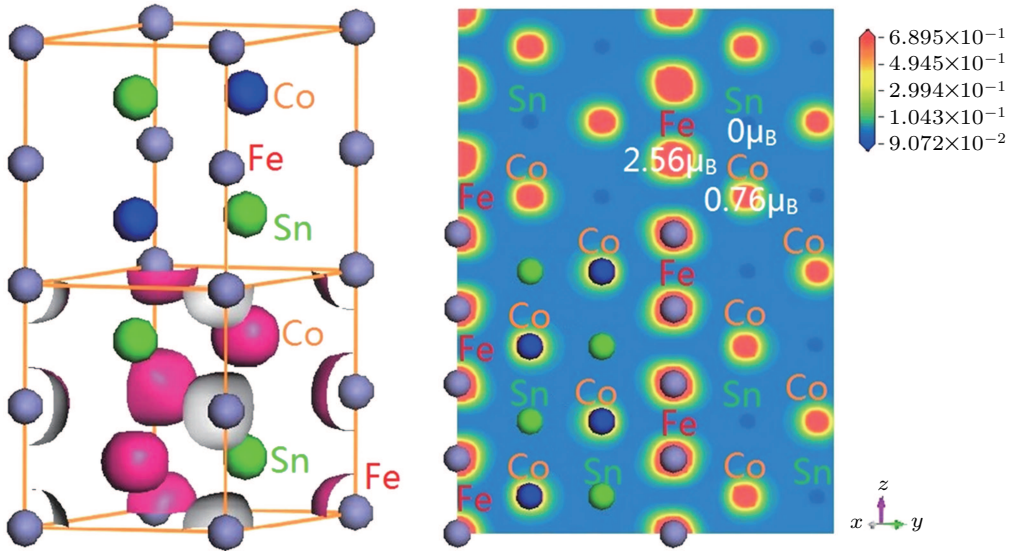



**Fig. 7.** (color online) The magnetization distribution and contours of spin electron density of stoichiometric FeCoSn.

## 4. Conclusions

The structural, magnetic properties and electronic structures of hexagonal FeCoSn compounds were investigated. The FeCoSn with as-annealed bulk and ribbon states both crystallize in hexagonal structure with a small amount of FeCo-rich secondary phase. The Curie temperatures are 251 K and 229 K and the values of magnetization are 2.57 $\mu_B$/f.u. and 2.94 $\mu_B$/f.u. at 5 K with field up to 50 kOe for AQ1273 and RQ1073 samples, respectively. The first-principles calculations indicate that stoichiometric FeCoSn is a ferromagnet. The densities of states show that the Fe atom carries the main magnetic moments and determines the electronic structure around the Fermi level. A peak of DOS at Fermi level corresponds to the instability of the stoichiometric compound and leads to the FeCo-rich secondary phase. This study provides the basic parameters of FeCoSn compound, especially for the tuning of the magneto-structural phase transitions.

## References

[1] Castelliz L 1953 *Monatsh. Chem.* **84** 765
[2] Szytuła A, Pędziwiatr A T, Tomkowicz Z and Bażeła W 1981 *J. Magn. Magn. Mater.* **25** 176
[3] Johnson V 1975 *Inorg. Chem.* **14** 1117
[4] Bażeła W, Szytuła A, Todorović J, Tomkowicz Z and Zięba A 1976 *Phys. Status Solidi A* **38** 721
[5] Szytuła A, Tomkowicz Z, Bażela W, Todorović J and Zięba A 1977 *Physica B & C* **93** 393
[6] Fjellvåg H and Andresen A F 1985 *J. Magn. Magn. Mater.* **50** 291
[7] Nizioø S, Bombik A, Bażeła W, Szytuła A and Fruchart D 1982 *J. Magn. Magn. Mater.* **27** 281
[8] Sandeman K G, Daou R, Ozcan S, Durrell J H, Mathur N D and Fray D J 2006 *Phys. Rev. B* **74** 224436
[9] Bażeła W, Szytuła A, Todorović J and Zięba A 1981 *Phys. Status Solidi A* **64** 367
[10] Zhu W, Feng L, Chen J L, Wang W H, Wu G H, Liu H Y, Meng F B, Luo H Z and Li Y X 2010 *Europhys. Lett.* **91** 17003
[11] Liu E K, Wang W H, Feng L, Zhu W, Li G J, Chen J L, Zhang H W, Wu G H, C B, Xu H B and d Boer F 2012 *Nat. Commun.* **3** 873
[12] Liu E K, Zhang H G, Xu G Z, Zhang X M, Ma R S, Wang W H, Chen J L, Zhang H W, Wu G H, Feng L and Zhang X X 2013 *Appl. Phys. Lett.* **102** 122405
[13] Wei Z Y, Liu E K, Li Y, Xu G Z, Zhang X M, Liu G D, Xi X K, Zhang H W, Wang W H, Wu G H and Zhang X X 2015 *Adv. Electron Mater.* **1** 1500076
[14] Li Y, Wei Z Y, Zhang H G, Liu E K, Luo H Z, Liu G D, Xi X K, Wang S G, Wang W H, Yue M, Wu G H and Zhang X X 2016 *APL Mater.* **4** 071101

[15] Koyama K, Sakai M, Kanomata T and Watanabe K 2004 *Jpn. J. Appl. Phys. Part 1* **43** 8036
[16] Barcza A, Gercsi Z, Knight K S and Sandeman K G 2010 *Phys. Rev. Lett.* **104** 247202
[17] Li G J, Liu E K, Zhang H G, Zhang Y J, Chen J L, Wang W H, Zhang H W, Wu G H and Yu S Y 2013 *J. Magn. Magn. Mater.* **332** 146
[18] Vaez A 2013 *J. Supercond. Nov. Magn.* **26** 1339
[19] Zhang C L, Han Z D, Qian B, Shi H F, Zhu C, Chen J and Wang T Z 2013 *J. Appl. Phys.* **114** 153907
[20] Zhang C L, Wang D H, Han Z D, Qian B, Shi H F, Zhu C, Chen J and Wang T Z 2013 *Appl. Phys. Lett.* **103** 132411
[21] Ma S C, Hou D, Yang F, Huang Y L, Song G, Zhong Z C, Wang D H and Du Y W 2014 *Appl. Phys. Lett.* **104** 202412
[22] Zeng J X, Wang Z L, Nie Z H and Wang Y D 2014 *Intermetallics* **52** 101
[23] Chen J H, Wei Z Y, Liu E K, Qi X, Wang W H and Wu G H 2015 *J. Magn. Magn. Mater.* **387** 159
[24] Ma S C, Su Y, Yang M, Yang F, Huang Y L, Liu K, Zhang L and Zhong Z C 2015 *J. Alloys Compd.* **629** 322
[25] Samanta T, Lepkowski D L, Saleheen A U, Shankar A, Prestigiacomo J, Dubenko I, Quetz A, Oswald I W H, McCandless G T, Chan J Y, Adams P W, Young D P, Ali N and Stadler S 2015 *J. Appl. Phys.* **117** 123911
[26] Zhang C L, Shi H F, Ye E J, Nie Y G, Han Z D and Wang D H 2015 *J. Alloys Compd.* **639** 36
[27] Liu J, Gong Y Y, Xu G Z, Peng G, Shah I A, Hassan N Ul and Xu F 2016 *Sci. Rep.* **6** 23386
[28] Ozono K, Mitsui Y, Umetsu R Y, Hiroi M, Takahashi K and Koyama K 2016 *AIP Conf. Proc.* **1763** 020003
[29] Ren Q Y, Hutchison W D, Wang J L, Studer A J, Md Din M F, Muñoz Pérez S, Cadogan J M and Campbell S J 2016 *J. Phys. D: Appl. Phys.* **49** 175003
[30] Kasimov D, Liu J, Gong Y Y, Xu G Z, Xu F and Lu G 2018 *J. Alloys Compd.* **733** 15
[31] Payne M C, Teter M P, Allan D C, Arias T A and Joannopoulos J D 1992 *Rev. Mod. Phys.* **64** 1045
[32] Perdew J P, Chevary J A, Vosko S H, Jackson K A, Pederson M R, Singh D J and Fiolhais C 1992 *Phys. Rev. B* **46** 6671
[33] Kanomata T and Goto T 1989 *Phys. Status Solidi A* **111** K1
[34] Bażela W, Szytuła A and Zając W 1981 *Solid State Commun.* **38** 875